Polarized Non-Line-of-Sight Imaging

Kenichiro Tanaka[1,2] Yasuhiro Mukaigawa[1] Achuta Kadambi[2]
[1]Nara Institute of Science and Technology (NAIST), Japan
[2]University of California, Los Angeles (UCLA), USA
{ktanaka, mukaigawa}@is.naist.jp achuta@ee.ucla.edu

Abstract

This paper presents a method of passive non-line-of-sight (NLOS) imaging using polarization cues. A key observation is that the oblique light has a different polarimetric signal. It turns out this effect is due to the polarization axis rotation, a phenomena which can be used to better condition the light transport matrix for non-line-of-sight imaging. Our analysis and results show that the use of a polarization for NLOS is both a standalone technique, as well as an enhancement technique to boost the results of other forms of passive NLOS imaging. We make a surprising finding that, despite 50% light attenuation from polarization optics, the gains from polarized NLOS are overall superior to unpolarized NLOS.

1. Introduction

Non-Line-of-Sight (NLOS) imaging is an active research topic in computational imaging. The goal is to visualize a scene that is hidden from the camera's line of sight, *e.g.*, "looking around the corners". Several prior works have tackled this problem, using methods that range from (a) time of flight imaging [49, 22, 33, 37, 32, 35, 46, 6, 17, 11, 52, 47, 36, 2]; (b) wave optics [25, 12, 11, 52]; (c) shadows [5, 44, 53, 3, 43]; and even (d) machine learning [42, 10, 8]. This paper takes a different tack, proposing the use of polarization cues to re-examine the NLOS problem.

Of particular interest is passive NLOS imaging where one is unable to control the probing illumination. Such limited programmable control makes scene reconstruction very challenging—existing passive NLOS methods [39] offer blurry reconstructions, as compared to active NLOS. This "blur" in existing passive NLOS methods can be mathematically linked to the scene's light transport matrix. To obtain better recovery, previous work aims to reduce the condition number of the light transport matrix. This has been done, for example, by placing a partial occluder in the scene to create high-frequency shadows [39].

Our method is analogous to prior approaches in passive NLOS, but we make a first attempt to use (linear) polarization cues to improve the conditioning of the light transport matrix. Our method creates high-frequency variation in the light transport matrix by, ideally placing the camera at the Brewster angle of polarization.

In this angle, the reflected light is linear polarized and can be analyzed by the polarizer. We also found that the polarizer's blocking axis varies depending on the oblique viewing angle and changes the intensity. We refer this effect as *effective angle* of polarizer. We show in the paper that this oblique observation provably changes the conditioning of the light transport matrix. Further, these benefits of polarization can apply to multiple configurations for passive NLOS. For example, polarization can be used to enhance occluder-based passive NLOS or direct passive NLOS imaging.

In summary, we make the following contributions:

- We bring the polarizer's effective angle theory to the computer vision field. The polarizer's transmitting/blocking axis depends on both zenith and azimuth angle of the light ray, which conveys rich angular information;
- We demonstrate that the polarization cues are able to improve the conditioning of the light transport for passive NLOS imaging without scene modifications; and
- We demonstrate that the same polarization cues also improve other passive NLOS approaches, including those that use partial occluders.

Scope: While polarization is a fresh signal for use in NLOS imaging, the quality of passive NLOS (after polarization enhancement) does not approach that of active methods, which have been shown to obtain extremely high-fidelity reconstructions. However, our polarization enhancement is fundamentally more general than the results we present here. A future extension details how the proposed technique could apply to active NLOS imaging, covered in the appendix.

2. Related Work

In this section, we briefly review the related work regarding NLOS imaging. For a more comprehensive review of NLOS imaging, the readers are directed to [27].

Active NLOS imaging. NLOS imaging was first proposed in the context of active, time-resolved imaging by Raskar and Davis [38]. Later work experimentally demonstrated and theoretically evolved these ideas through the use of time of flight imagers, in particular streak cameras [49, 48, 22, 33], amplitude-modulated continuous-wave cameras [16, 20, 19], and single photon avalanche diodes (SPAD) and SPAD cameras [37, 32, 35, 46, 6, 17, 11, 52, 47, 36, 2]. There are other methods of performing active NLOS imaging that do not require time resolved information. For example, a coherent light source reveals occluded cues [4]. An object movement can also be tracked by speckle [40] or synthesis-based approaches [23]. Recent work has used a standard RGB camera and laser source to realize active NLOS [10]. Ding *et al*. [13] analyze the polarized light reflection to separate specular and diffuse reflection on the LOS wall. While active illumination increases the scene information, we choose to focus on enhancing the lower-performing, but more flexible configuration of passive NLOS imaging.

Passive NLOS imaging There are fewer works that study the hard problem of passive NLOS. One promising approach is to use shadows and corners. Bouman *et al*. [5] use the high-frequency detail of a corner to track occluded scenes (this work is partially inspired by accidental pinhole cameras [44]). An extension of this is proposed in [39, 53, 15], where a partial obstacle is placed between the wall and NLOS scene. An orthogonal approach is to image thermal scenes around the corner. Here, heat is passively emitted by the human body, which simplifies the NLOS problem to a 1-bounce reflection, enabling high-quality video of a human figure, in real-time [28, 21]. Our technique is complementary, as polarization can enhance the quality of most methods referenced above.

Analysis of NLOS imaging The recoverability of NLOS imaging depends on many factors. Kadambi *et al*. [20] propose the first bound on the spatial resolution of NLOS imaging, and in particular active NLOS. Liu *et al*. [24] analyze the feature visibility of SPAD-based NLOS imaging. Saunders *et al*. [39] analyze the aperture of NLOS imaging using the size of the LOS wall and the obstacles. Pediredla *et al*. [36] propose a temporal focusing using ellipsoidal projection. In this paper, we follow the structure of previous techniques in analyzing how the condition number of the light transport matrix is favorably modified through the use of polarization cues.

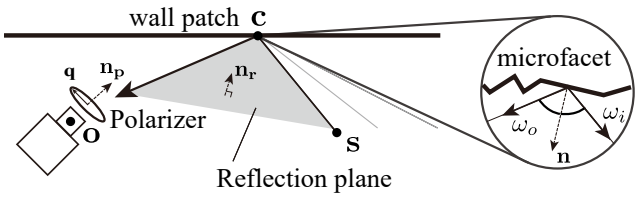

Figure 1: **Diagram of the geometry of the problem.** The camera is looking at the wall and the scene point is out of sight of the camera. On a microfacet model, each reflection path can be considered as a sum of mirror reflections, hence the polarization is preserved.

Polarization cues Polarization cues can be used for 3D geometry recovery [18, 31, 51, 9, 26] and imaging through scattering media [45, 41, 14]. We firstly use the polarization cues for enhancing passive NLOS imaging.

Polarizer at oblique view In the LCD development field, the light leakage of polarizer from oblique view is a major problem [54, 34]. While they aim to cancel this effect, we bring this effect to improve the NLOS imaging problem.

3. Light Transport: Passive NLOS Imaging

Suppose a camera is pointed toward the line-of-sight (LOS) wall and the scene is non-line-of-sight (NLOS) to the camera as shown in Fig. 1. Without loss of generality, we consider that the NLOS scene is a set of point light sources. Then, the intensity $I(\mathbf{c})$ at the wall patch $\mathbf{c}$ is given by

$$I(\mathbf{c}) = \iint_{\mathbf{s}\in\mathcal{S}} T(\mathbf{s},\mathbf{c}) l(\mathbf{s}) d\mathbf{s}, \tag{1}$$

where $\mathbf{s}$ is a point in the scene $\mathcal{S}$, $l(\mathbf{s})$ is the intensity of the scene point $\mathbf{s}$, and $T(\mathbf{s},\mathbf{c})$ is the light transport from the scene point $\mathbf{s}$ to the camera via the wall patch $\mathbf{c}$. The model can be discretized as

$$\mathbf{i} = \mathbf{T}\mathbf{l}, \tag{2}$$

where $\mathbf{i}$ is the vectorized observations, $\mathbf{T}$ is the light transport matrix, and $\mathbf{l}$ is the vectorized scene intensities. If the light transport matrix is known or generatable, the NLOS intensities can be estimated by least squares sense as

$$\hat{\mathbf{l}} = \mathbf{T}^{+}\mathbf{i}, \tag{3}$$

where $\mathbf{T}^{+}$ is the pseudo-inverse matrix of $\mathbf{T}$. The stability of solving this linear system depends on how small the condition number of the matrix is. A key goal of previous methods has been to improve the conditioning of Eq. (3).

Previous methods of conditioning Eq. (3): Perhaps the simplest way to decrease the condition number is to use a favorable bidirectional reflectance distribution function (BRDF). A trivial case is the mirror, which makes the lowest condition number because the light transport matrix becomes identity. An opposite example is the diffuse wall, which makes a very large condition number because the single light source contributes to the all camera pixels. The conditioning of using other materials that have specularity are between the mirror and the diffuse wall because they somehow preserve high frequency component. Extended discussion on this topic can be found in [20]. Another way to improve the conditioning is to place obstacles in the scene, such as putting a partial obstacle between the wall and the scene. Saunders *et al*. [39] place an arbitrary obstacle between the camera and the wall to block the light rays. This makes a shadow on the wall, which contains high-frequency information. For more detail, the readers are referred to papers that use obstacles [39, 53, 15]. Both of these approaches modify the scene.

4. Light Transport: Polarized NLOS Imaging

We aim to minimize modifications to the scene for conditioning Equation 3 using polarization. Hence, we only use a polarizer at the camera side. This approach is also able to conditioning the existing method using partial occluders. If putting a partial occluder to the scene is tolerable, combining the existing method and the proposed method improves the conditioning further.

By putting a polarizer in front of the camera, a small angular difference of light paths makes a big intensity variance, thus the conditioning is improved compared to a normal observation without polarizer. A key observation of this paper is that the polarizer's effective axis is slightly rotated if the light ray is oblique to the polarizer. In other words, the perpendicular light rays are blocked while oblique light rays pass through the polarizer. In the following section, we reveal how the polarization light transport is modeled in passive NLOS imaging.

Polarized NLOS scenes If the NLOS scene itself is polarized, then we can exploit cross-polarization effects to improve the NLOS problem even more. Further detail is deferred to the supplementary material.

4.1. Effective angle of polarizer

We introduce the effective angle of a polarizer, which is well studied in the area of LCD development [54, 34]. When the light ray is oblique to the polarizer, the light is 'leaked' even if two linear polarizers are put crossed. This is because the effective polarization axis of the polarizer depends on the azimuth and zenith angle of the incident light ray. Figure 2(a, b) shows pictures of the same scene from top and oblique views. While the light from the LCD is blocked on the top view, the content of the LCD is slightly visible from oblique view even though the polarizer is put crossed. This effect is angle dependent, therefore it can be used for analyzing NLOS observations.

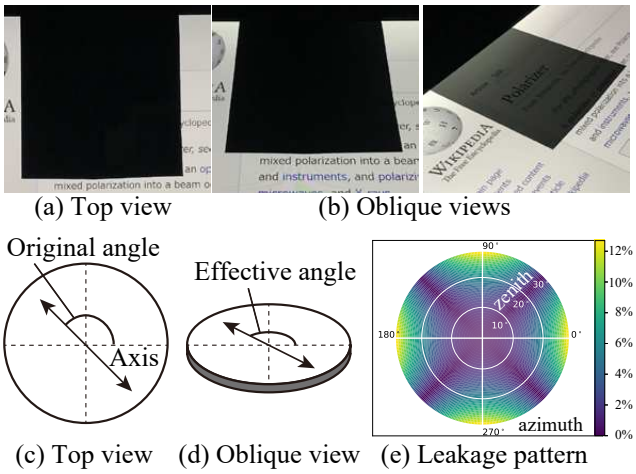

Figure 2: **Polarizer from oblique view.** While the LCD monitor is invisible from top view (a), it is slightly visible from certain oblique views depending on the zenith and azimuth angles (b). (c) The original angle of polarizer from top view. (d) The effective angle from oblique view. The polarizer axis is slightly declined. (e) Light leakage pattern of crossed polarizers from oblique view. These polarizers' original angles are $45°$ and $-45°$, respectively.

Light leakage occurs because the effective angle of the polarizer changes due to the light ray's azimuth and zenith angles. From a geometrical calculation[1], the effective angle θ' from the incident light viewpoint is represented as

$$\tan\theta' = -\frac{\cos(z)}{\tan(\theta - a)}, \tag{4}$$

where θ is the original polarizer's axis, *i.e*., the polarizer's axis from top view, a and z are azimuth and zenith angles of the incident ray, respectively. As θ' is the angle between the polarizer and the polarized light, it is wrapped between 0 and $\pi/2$. Figure 2(c - e) shows the original and effective angles of polarizers and the light leakage pattern of crossed polarizers. This pattern can be utilized to improve the NLOS imaging.

4.2. Polarization light transport on rough surface

Now, we consider the polarization light transport model on a rough surface. In this paper, we employ a microfacet model for the rough surface, shown in the inset of

[1]Refer to supplementary material for additional details.

Fig. 1. The surface normal of each facet that reflects the light source to the camera is identical to the half vector of the viewing and lighting vectors. Therefore, the light transport $T(\mathbf{s}, \mathbf{c})$ from the scene point $\mathbf{s}$ to the camera via the wall patch $\mathbf{c}$ is represented as

$$T(\mathbf{s}, \mathbf{c}) = \Omega(\boldsymbol{\omega_i}, \boldsymbol{\omega_o})\lambda(\boldsymbol{\omega_i}, \boldsymbol{\omega_o}, \mathbf{q}), \tag{5}$$
$$\begin{cases} \boldsymbol{\omega_i} & = \frac{\mathbf{s}-\mathbf{c}}{\|\mathbf{s}-\mathbf{c}\|_2}, \\ \boldsymbol{\omega_o} & = \frac{\mathbf{o}-\mathbf{c}}{\|\mathbf{o}-\mathbf{c}\|_2}, \end{cases}$$

where Ω is the BRDF of the rough surface, $\boldsymbol{\omega_o}$ is the viewing vector, $\boldsymbol{\omega_i}$ is the incident vector, $\mathbf{o}$ is the camera position, λ is the light leaking/blocking effect due to polarizer, and $\mathbf{q}$ is the polarizer's axis. The polarizer modulates light transport by introducing the leakage term λ, which makes the improvement to the light transport matrix.

As we assume the microfacet model, the reflection on each facet can be modelled as a Fresnel reflection. The Fresnel reflection is known to be partially polarized and reflectances of s and p polarization components R_s and R_p can be represented as

$$R_p(\phi) = \frac{\tan^2(\phi - \phi')}{\tan^2(\phi + \phi')}, \tag{6}$$

$$R_s(\phi) = \frac{\sin^2(\phi - \phi')}{\sin^2(\phi + \phi')}, \tag{7}$$

$$\phi' = \sin^{-1}\frac{\sin(\phi)}{\eta}, \tag{8}$$

where ϕ is the incident angle, ϕ' is the refractive angle, and η is the refractive index of the wall.

When the incident and reflection angle is at Brewster angle, the reflected light is completely linearly polarized. This is because the reflectance of p polarization becomes zero. By putting the camera at near the Brewster angle position as shown in Fig. 3, highly polarized observations can be obtained, thus the observation can be analyzed with a polarizer in front of the camera.

Placing a polarizer in front of the camera such that the polarized reflection is blocked at a specific light path, leads to the observation of a light leakage pattern. Because the other light paths from neighboring wall points are oblique to the polarizer's blocking axis, the leakage pattern can be observed as shown in the right of Fig. 3.

The leakage pattern λ can be modeled as

$$\lambda(\boldsymbol{\omega_i}, \boldsymbol{\omega_o}, \mathbf{q}) = R_p(\theta_h)\cos(\theta') + R_s(\theta_h)\sin(\theta'), \tag{9}$$
$$\begin{cases} \theta_h & = \frac{1}{2}\cos^{-1}(\boldsymbol{\omega_o} \cdot \boldsymbol{\omega_i}) \\ \theta' & = \tan^{-1}\left(-\frac{\cos(z)}{\tan(\theta - a)}\right) \\ z & = \cos^{-1}(-\boldsymbol{\omega_o}\mathbf{n_p}) \\ \theta - a & = \cos^{-1}(-\mathbf{wq}) \\ \mathbf{w} & = \frac{\boldsymbol{\omega_o} + \cos(z)\mathbf{n_p}}{\|\boldsymbol{\omega_o} + \cos(z)\mathbf{n_p}\|_2} \end{cases}$$

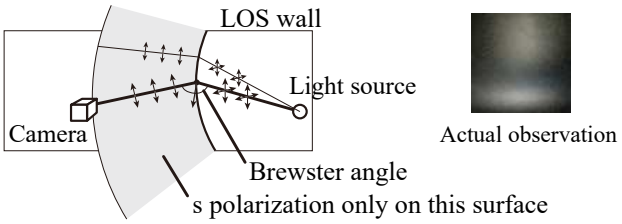

Figure 3: **The Brewster angle geometry.** Putting the camera so that light path is at Brewster angle, only one directional polarization (s polarization component) is reflected to the camera. Because there is no effect from p polarization, it is possible to observe a light leakage pattern only using a polarizer in front of the camera. The right image is the actual observation of the reflection of a unpolarized point light source.

where $\mathbf{q}$ is the polarizer's axis, θ_h is the half angle of the reflection path, θ' is the effective angle of the polarizer, and $\mathbf{n}_p$ is the normal of the polarizer.

Combination with the existing method Polarization light transport can be combined with existing method such as putting partial occluder in the scene [39]. The light transport matrix in this case becomes

$$T(\mathbf{c}, \mathbf{s}) = T'(\mathbf{c}, \mathbf{s})\lambda(\boldsymbol{\omega_i}, \boldsymbol{\omega_o}, \mathbf{q}), \tag{10}$$

where T' is the light transport matrix of the existing method. Again, the difference is the existence of λ and this improves the condition number of the light transport matrix.

4.3. Other factors

Polarized scene Although most NLOS scenes are unpolarized, in the rare cases where the NLOS scene is polarized, our method is extremely advantageous. Consider that if the scene is polarized such as an LCD monitor, Eq. (9) can be rewritten as

$$\lambda(\boldsymbol{\omega_i}, \boldsymbol{\omega_o}, \mathbf{q}) = I_p R_p(\theta_h)\cos(\theta') + I_s R_s(\theta_h)\sin(\theta'), \tag{11}$$

where I_p and I_s is the intensity of p and s polarization components of the scene. Here, it is possible to place the polarizer at an angle where one of the polarization components becomes zero. Therefore, there is no restriction of having the capture setup oriented to the Brewster angle, as in the general case we have described above. We expand on this discussion in the supplement, and show results.

Why not rotate the polarizer? This paper relies on taking 1 image from a polarization filter at 90 degrees (parallel to the reflection plane). A natural question is whether

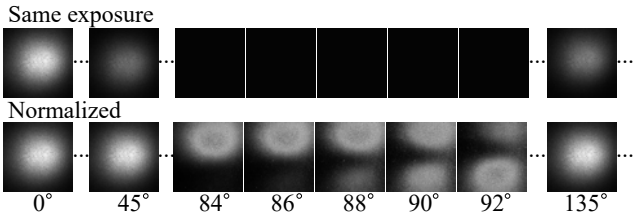

Figure 4: **Comparison to rotating the polarizer.** The upper row is the captured images of the same exposure time, and the lower images are normalized at each maximum value. The dark band, where the light is completely blocked by polarizer, is a key observation and only appears around 90 degrees.

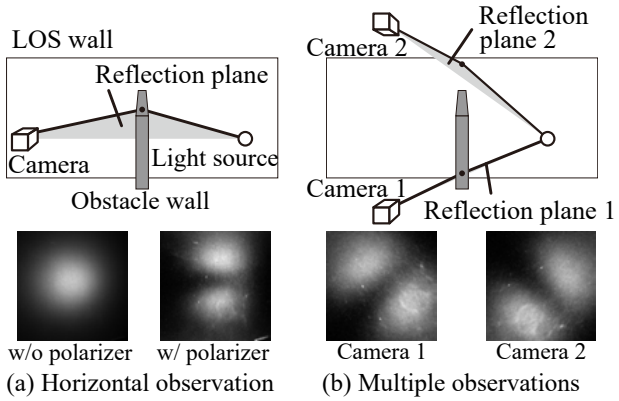

Figure 5: **Camera position and reflection plane.** (a) Using a single camera position, only one direction is encoded in the image. The intensity variance of horizontal direction is not so improved. (b) Using multiple camera positions, the scene can be encoded by multiple directions.

the filter can be rotated to take multiple pictures. Since we rely on a leakage pattern, there is little benefit to capturing multiple images, as the variation in polarization images at angles other than 90 degrees is subtle, while the capture effort increases linearly. Very specifically, the key improvement from using polarizers comes from the 'dark band' in the image as shown in Fig. 4. Figure 4 shows the observation image while rotating the polarizer and without the polarizer. The dark band, where the light is blocked, appears only around 90 degrees, while other angles look similar to the image without the polarizer.

Multiple camera positions The leakage pattern appears parallel to the reflection plane. Figure 5(a) shows the actual measurement of the wall, where the scene is a point light source. There is large intensity variance in the vertical direction, and therefore the vertical information is better preserved. On the other hand, the horizontal intensity variance

Standalone

	w/o	rotating	single	**multiple**
Cond. num.	686.8	486.3	357.0	**327.9**
Percentage	–	70.8%	52.0%	**47.7%**

With partial occluder

	w/o	rotating	single	**multiple**
Cond. num.	172.3	170.6	146.1	**113.9**
Percentage	–	99.0%	84.8%	**66.1%**

Table 1: **Condition number comparison.** Methods without polarizer, rotating polarizer, crossed polarizer from a single camera position, and crossed polarizer from multiple camera positions are compared. Our method has the lowest condition number.

is lower and likely to the unpolarized observations. To overcome the slim variance in the horizontal direction, it is possible to capture the scene from multiple camera positions, enabling the capture of perpendicular reflection planes as shown in Fig. 5(b).

5. Simulation

Our simulations verify that polarization leakage can be used to improve the condition number of the light transport matrix.

Condition number The effectiveness of the method is confirmed by examining the condition number of light transport matrices. The lower condition number gives better recovery quality. The camera and the light source are placed 10 cm from the wall. The image is 7×7 pixels and the scene is 3×3 pixels, so the matrix is 49×9. The light sources are placed on a plane and not polarized. For a single image observation, the geometry of Fig. 5(a) is selected, and for multiple camera settings, the geometry of Fig. 5(b) is used. The condition number for each setting is summarized in Table 1. Our method has the smallest condition number, indicating the potential for about two times better recoverability. Likewise, we also show the case when there is a partial occluder in the same table. We observe through simulation that the condition number is improved using a polarizer as well.

Improvement w.r.t. wall roughness The effectiveness of this method depends on the type of the wall. To confirm this, the improvement in condition number is evaluated while changing the roughness of the wall. The roughness is changed from 0 (mirror-like) to 1 (completely diffuse). The plot of the condition number and improvement ratio is shown in Fig. 6. For all roughness parameters, it is observed that the polarization cues improve the condition number.

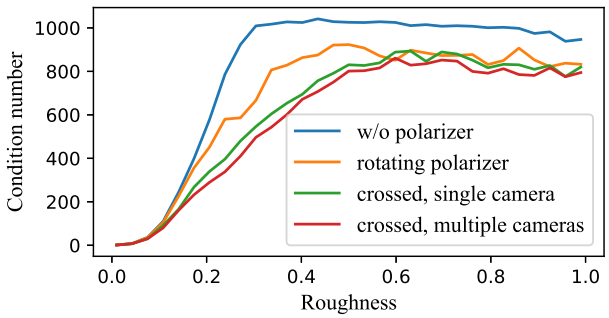

Figure 6: **Condition number with respect to the roughness of the wall.** Lower the better. The roughness ranges 0 (mirror-like) to 1 (diffuse-like). Our method has the lowest condition number for all roughness parameter.

Although the plots of single and multiple cameras look similar, we observe that the multiple camera setting is always slightly better than single camera setting. When the roughness decreases, the wall becomes mirror-like and there is no improvement using a polarizer because the NLOS scene is originally visible. The best performance is observed at the middle of specular and diffuse reflections, where a lot of materials have such specularities [30].

6. Experiment

Real experiments are consistent with simulations: polarization improves NLOS image reconstruction. For all following experiments, we use ADMM to solve Eq. (2), consisting of a 2D total variation regularizer with a box constraint. For clarity, we estimate

$$\hat{\mathbf{l}} = \underset{\mathbf{l}}{\operatorname{argmin}} \|\mathbf{i} - \mathbf{T}\mathbf{l}\|_2^2 + \lambda TV_{2\mathrm{D}}(\mathbf{l}) \qquad (12)$$
$$\text{s. t.} \quad 0 \preceq \mathbf{l} \preceq 1.$$

Because this is a convex optimization problem, it can be solved in a polynomial time. For all cases, the BRDF of the wall is measured beforehand.

Polarized NLOS Firstly, we evaluate the polarized NLOS without partial occluder. For numerical evaluation of non-polarized scene, a projector is used to project the scene image. Figure 7 shows the setup and the result. Two images are compared with and without the polarizer in front of the camera. While it is difficult to see the projected scenes if the polarizer is not used, the scene is visible using the polarizer. We also projected more images, which can be found in the supplementary material. The table shows the numerical evaluation of the results. Peak signal to noise ration (PSNR), zero-mean normalized cross correlation (ZNCC), and structural similarity (SSIM) are used. It is confirmed

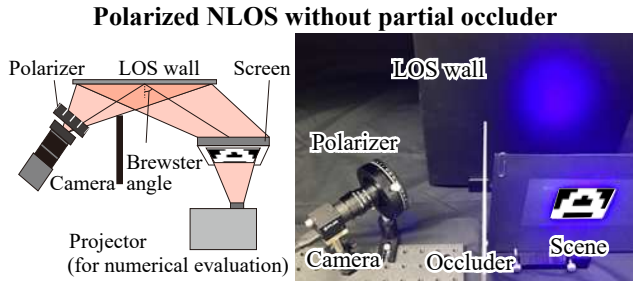

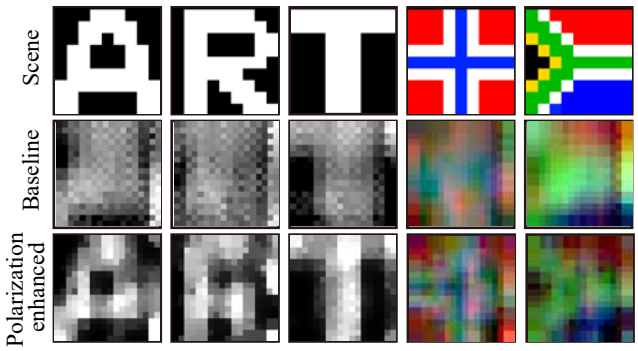

	Baseline	Polarization enhancement
condition number	2961	**2012**
PSNR	6.7 dB	**7.3 dB**
ZNCC	0.45	**0.65**
SSIM	0.25	**0.28**

Figure 7: **Polarized NLOS results without occluder.** A projector is used for numerical evaluation and to make the scene unpolarized. The scene is recovered with and without the polarizer in front of the camera. Using polarization, the recovered images are improved. Improvement is confirmed by comparing condition number and three image measures.

that the condition number is decreased and the recovered image is improved for every image metric if the polarization is used.

Polarized NLOS w/ partial occluder for reflective objects Here, we show that Polarized NLOS can also enhance existing techniques. As shown in Fig. 8 *top-left*, we reproduce the partial occluder method from Saunders *et al*. [39]. Reflective object scenes are recovered in this experiment and enhanced by polarization. Figure 8 shows the setup, the target object, the recovered result by the existing method, and the enhanced result by polarization. The target object is lit by an uncontrolled light source. In the results of the baseline method, it is difficult to see the resolution chart and the content of the book. On the other hand, our technique recovers images with higher contrast. The clear texture of resolution chart and printed materials are visualized in detail. The observed image is 160×100 pixels and

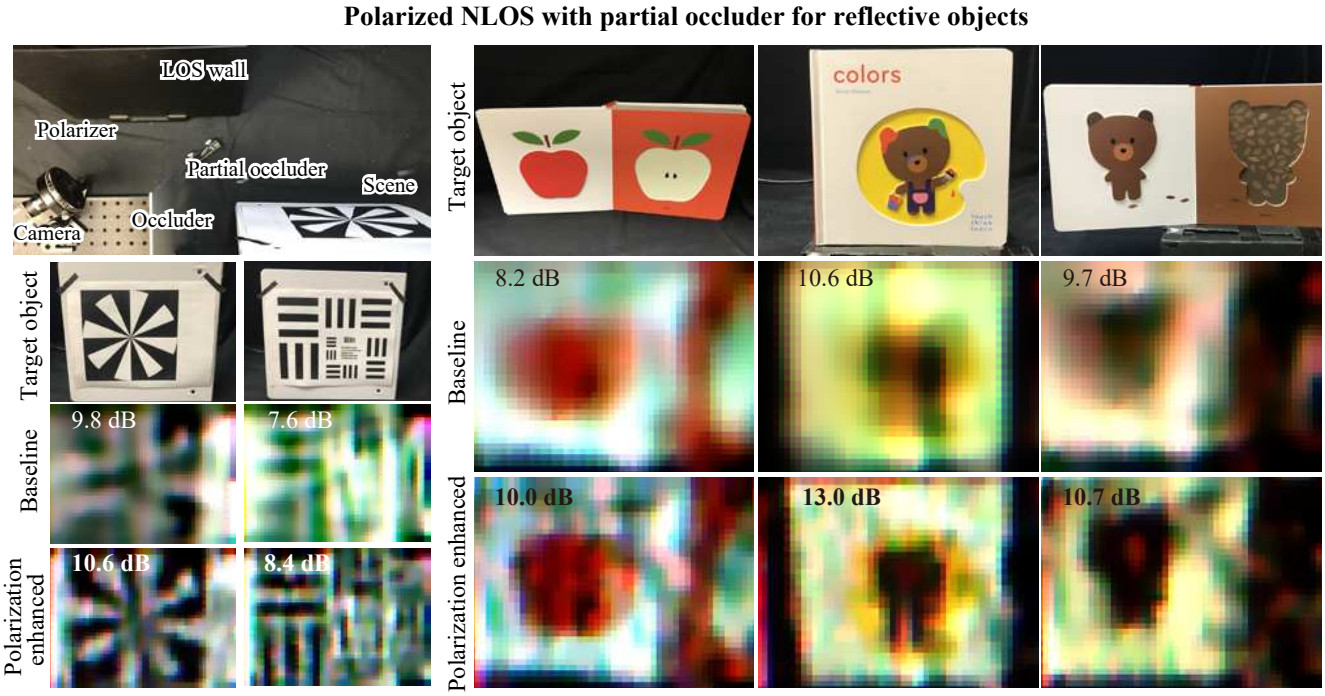

Figure 8: **Results for reflective objects.** *Top-left:* the setting of the experiment. The scene is a reflective object (not self-luminous). *1st row:* The photograph of target objects. *2nd row:* The recovered images by the baseline method [39]. *Bottom row:* The recovered images by our method. High frequency details are recovered. Clear detail of resolution charts, sharp edge of apple, and the detailed shape of bears are clearly visualized. PSNR values are calculated with homography-transformed photograph for reference.

the scene is 56×40 pixels, so the matrix is 16000×2240. The exposure is 5 seconds. The processing time to solve Eq. (12) takes approximately 1.5 seconds. Our method quantitatively and qualitatively improves the reconstruction. We provide more diverse scenes in the supplement.

Comparing our enhancement to image processing An interesting question that is raised is whether the performance improvements we obtain could be achieved by applying image post-processing algorithms to conventional NLOS (without polarization). Figure 9 shows the result of projected images and also includes the result of applying image post-processing. The baseline method in this case is [39]. Here, a total variation (TV) denoising algorithm [7][2] and a deep learning image processor (neural enhance) [1] are used. While the image is improved by post processing, it is impossible to recover the higher frequency component that is lost on the wall reflection, because recovering lost information is mathematically impossible. On the other hand, our method recovers higher frequency detail, which is preserved by polarization light transport. PSNR, ZNCC, and SSIM values show significant improvement.

[2]We tried several denoising algorithms and report the best for comparison (TV denoising).

7. Discussion

In summary, there are two surprising findings from this paper. The *first surprising finding* is that polarized NLOS has superior results to ordinary NLOS. The finding is a surprise as initially we were not sure if any method could overcome the 50% light loss inherent to using a polarization filter. We are cautiously optimistic, now that this paper has surpassed the break-even point by a considerable margin. The *second surprising finding* is that our polarization paper does not actually leverage the rotation angle of the polarizing filter. In contrast, we use the principle of leakage, observed when one views an liquid crystal display off-axis.

Our method is not without assumptions, though our practical results substantiate the validity of our assumptions. For instance, we assume that the wall preserves polarization. This holds for many rough surfaces, although for certain surfaces the signal can be subtle. Concretely, walls that have a dominant subsurface scattering, such as plastic and plaster, can be more challenging because one loses the polarization property, i.e., the ratio of polarization due to Fresnel reflection becomes low. In the future, we might seek to

combine rotational and angular effects of polarizing filters, where the former has been shown to be a driving force for 3D scene geometry [18]. In addition, we may also leverage polarized event cameras [29, 55, 50] to identify the subtle signal.

In conclusion, we believe that, despite the 50 percent light loss, polarization can enhance a large swath of NLOS imaging methods. As shown in the appendix, the proposed method can be extended to active NLOS imaging techniques as well. We hope this paper spurs interest in using polarization as an additional tool in NLOS imaging.

Appendix: On Active NLOS Imaging

Followed by the previous work [2, 16, 35, 22, 49], an active NLOS imaging using time-of-flight measurement can be modeled as

$$i(t;\mathbf{p},\mathbf{c}) = \iiint_{\mathbf{s}\in\mathcal{S}} \rho(\mathbf{s}) \frac{\delta(\|\mathbf{s}-\mathbf{p}\| + \|\mathbf{s}-\mathbf{c}\| - ct)}{\|\mathbf{s}-\mathbf{p}\|^2 \|\mathbf{s}-\mathbf{c}\|^2} \times \Omega(\boldsymbol{\omega}_{\mathbf{i}l}, \boldsymbol{\omega}_{\mathbf{o}l}) \Omega(\boldsymbol{\omega}_{\mathbf{i}c}, \boldsymbol{\omega}_{\mathbf{o}c}) d\mathbf{s}, \quad (13)$$

$$\begin{cases} \boldsymbol{\omega}_{\mathbf{i}l} &= \frac{\mathbf{s}-\mathbf{p}}{\|\mathbf{s}-\mathbf{p}\|_2}, \\ \boldsymbol{\omega}_{\mathbf{o}l} &= \frac{\mathbf{o}-\mathbf{p}}{\|\mathbf{o}-\mathbf{p}\|_2}, \\ \boldsymbol{\omega}_{\mathbf{i}c} &= \frac{\mathbf{s}-\mathbf{c}}{\|\mathbf{s}-\mathbf{c}\|_2}, \\ \boldsymbol{\omega}_{\mathbf{o}c} &= \frac{\mathbf{o}-\mathbf{c}}{\|\mathbf{o}-\mathbf{c}\|_2}, \end{cases}$$

where $i(t;\mathbf{p},\mathbf{c})$ is the temporal transient observation at the wall patch $\mathbf{c}$ by illuminating the wall patch $\mathbf{p}$ by a pulsed light, ρ is the 3D NLOS albedo, δ is the Dirac delta function, c is the speed of light, and Ω is the BRDF of the LOS wall. Discretizing, we obtain

$$\mathbf{i} = \mathbf{T}\boldsymbol{\rho}, \quad (14)$$

where $\mathbf{T}$ is the light transport matrix of active NLOS model and $\boldsymbol{\rho}$ is the vectorized NLOS albedo.

Analogous to the passive case, when we put a polarizer in front of the camera, Eq. (13) is altered as

$$i'(t;\mathbf{p},\mathbf{c}) = \iiint_{\mathbf{s}\in\mathcal{S}} \rho(\mathbf{s}) \frac{\delta(\|\mathbf{s}-\mathbf{p}\| + \|\mathbf{s}-\mathbf{c}\| - ct)}{\|\mathbf{s}-\mathbf{p}\|^2 \|\mathbf{s}-\mathbf{c}\|^2} \times \Omega(\boldsymbol{\omega}_{\mathbf{i}l}, \boldsymbol{\omega}_{\mathbf{o}l}) \Omega(\boldsymbol{\omega}_{\mathbf{i}c}, \boldsymbol{\omega}_{\mathbf{o}c}) \lambda(\boldsymbol{\omega}_{\mathbf{i}c}, \boldsymbol{\omega}_{\mathbf{o}c}, \mathbf{q}) d\mathbf{s}, \quad (15)$$

where the light transport is modulated by the leakage term λ. Note that the polarization state of active light source is ignored because the light is assumed to be depolarized at the NLOS scene reflection.

Simulation We confirm the effectiveness of polarized NLOS for active NLOS imaging through a simulation. Figure 10 shows the condition number of the light transport matrix changing with scene configurations including wall's roughness parameter and the spatial resolution of NLOS scene. For all configurations, polarization cues improve the conditioning of the active NLOS imaging.

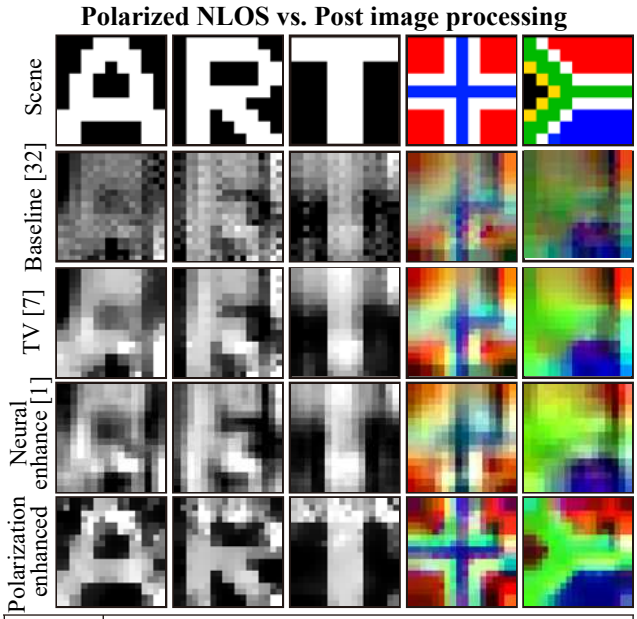

	Baseline [32]	TV [7]	Neural [1]	Polarization
PSNR	7.2 dB	8.8 dB	8.4 dB	**11.7 dB**
ZNCC	0.50	0.66	0.61	**0.87**
SSIM	0.29	0.37	0.31	**0.43**

Figure 9: **Polarized NLOS exceeds the quality of conventional NLOS with image processing.** The results of polarized NLOS with partial occluders. The result of the baseline method [39], TV denoised [7], image enhancement by neural network [1], and the result of our method are compared.

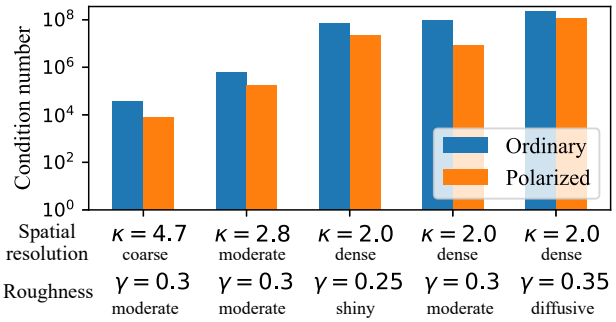

Figure 10: **Condition number of active NLOS.** The condition number of active setting is compared. The spatial resolution κ and the wall's roughness γ are changed. Using the polarization cues, the condition number is improved in the active setting for multiple scene configurations.

Acknowledgments This work is partly supported by JSPS Kaken JP18H03265. Achuta Kadambi is supported by an NSF Research Initiation Award (IIS 1849941), and a Young Faculty Award from Sony Imaging.

References

[1] *Neural Enhance*, Date accessed: Nov. 13th, 2019. https://github.com/alexjc/neural-enhance. 7, 8

[2] Byeongjoo Ahn, Akshat Dave, Ashok Veeraraghavan, Ioannis Gkioulekas, and Aswin C. Sankaranarayanan. Convolutional approximations to the general non-line-of-sight imaging operator. In *The IEEE International Conference on Computer Vision*, October 2019. 1, 2, 8

[3] Manel Baradad, Vickie Ye, Adam B. Yedidia, Frédo Durand, William T. Freeman, Gregory W. Wornell, and Antonio Torralba. Inferring light fields from shadows. In *2018 IEEE/CVF Conference on Computer Vision and Pattern Recognition*, pages 6267–6275, June 2018. 1

[4] Andre Beckus, Alexandru Tamasan, and George K. Atia. Multi-modal Non-line-of-sight passive imaging. *arXiv*, pages 1–10, 2018. 2

[5] Katherine L. Bouman, Vickie Ye, Adam B. Yedidia, Fredo Durand, Gregory W. Wornell, Antonio Torralba, and William T. Freeman. Turning corners into cameras: Principles and methods. In *IEEE International Conference on Computer Vision*, pages 2289–2297. IEEE, Oct 2017. 1, 2

[6] Mauro Buttafava, Jessica Zeman, Alberto Tosi, Kevin Eliceiri, and Andreas Velten. Non-line-of-sight imaging using a time-gated single photon avalanche diode. *Optics Express*, 23(16):20997, Aug 2015. 1, 2

[7] Antonin Chambolle. An algorithm for total variation minimization and applications. *Journal of Mathematical Imaging and Vision*, 20:89–97, 2004. 7, 8

[8] Sreenithy Chandran and Suren Jayasuriya. Adaptive lighting for data-driven non-line-of-sight 3d localization and object identification. *arXiv*, May 2018. 1

[9] Tongbo Chen, Hendrik P A Lensch, Christian Fuchs, and Hans Peter Seidel. Polarization and phase-shifting for 3D scanning of translucent objects. In *IEEE Computer Society Conference on Computer Vision and Pattern Recognition*, 2007. 2

[10] Wenzheng Chen, Simon Daneau, Fahim Mannan, and Felix Heide. Steady-state non-line-of-sight imaging. In *IEEE Conference on Computer Vision and Pattern Recognition*, pages 6790–6799. IEEE, 2019. 1, 2

[11] David B. Lindell, Gordon Wetzstein, and Matthew O'Toole. Wave-based non-line-of-sight imaging using fast f-k migration. *ACM Transactions on Graphics*, 38(4):116, 2019. 1, 2

[12] David B. Lindell, Gordon Wetzstein, and Vladlen Koltun. Acoustic non-line-of-sight imaging. In *IEEE Conference on Computer Vision and Pattern Recognition*, 2019. 1

[13] Yitian Ding, Ronan Kerviche, Amit Ashok, and Stanley Pau. Eavesdropping of display devices by measurement of polarized reflected light. *Applied Optics*, 57(19):5483–5491, 2018. 2

[14] Julien Fade, Swapnesh Panigrahi, Anthony Carré, Ludovic Frein, Cyril Hamel, Fabien Bretenaker, Hema Ramachandran, and Mehdi Alouini. Long-range polarimetric imaging through fog. *Applied Optics*, 53(18), 2014. 2

[15] Felix Heide, Matthew O'Toole, Kai Zang, David B. Lindell, Steven Diamond, and Gordon Wetzstein. Non-line-of-sight imaging with partial occluders and surface normals. *ACM Transactions on Graphics*, 38(3):1–10, May 2019. 2, 3

[16] Felix Heide, Lei Xiao, Wolfgang Heidrich, and Matthias B. Hullin. Diffuse mirrors: 3D reconstruction from diffuse indirect illumination using inexpensive time-of-flight sensors. In *IEEE Conference on Computer Vision and Pattern Recognition*, 2014. 2, 8

[17] Julian Iseringhausen and Matthias B. Hullin. Non-line-of-sight reconstruction using efficient transient rendering. *arXiv*, Sep 2018. 1, 2

[18] Achuta Kadambi, Vage Taamazyan, Boxin Shi, and Ramesh Raskar. Polarized 3D: High-Quality Depth Sensing with Polarization Cues. In *IEEE International Conference on Computer Vision*, pages 3370–3378. IEEE, Dec 2015. 2, 8

[19] Achuta Kadambi, Refael Whyte, Ayush Bhandari, Lee Streeter, Christopher Barsi, Adrian Dorrington, and Ramesh Raskar. Coded time of flight cameras: Sparse deconvolution to address multipath interference and recover time profiles. *ACM Transactions on Graphics*, 32(6):1–10, Nov 2013. 2

[20] Achuta Kadambi, Hang Zhao, Boxin Shi, and Ramesh Raskar. Occluded imaging with time-of-flight sensors. *ACM Transactions on Graphics*, 35(2):1–12, Mar 2016. 2, 3

[21] Masaki Kaga, Takahiro Kushida, Tsuyoshi Takatani, Kenichiro Tanaka, Takuya Funatomi, and Yasuhiro Mukaigawa. Thermal non-line-of-sight imaging using diffuse and specular reflections. *IPSJ Transactions on Computer Vision and Applications*, 11:1–6, 2019. 2

[22] Ahmed Kirmani, Tyler Hutchison, James Davis, and Ramesh Raskar. Looking around the corner using ultrafast transient imaging. *International Journal of Computer Vision*, 95(1):13–28, June 2011. 1, 2, 8

[23] Jonathan Klein, Christoph Peters, Jaime Martín, Martin Laurenzis, and Matthias B. Hullin. Tracking objects outside the line of sight using 2D intensity images. *Scientific Reports*, 6(1):32491, Oct 2016. 2

[24] Xiaochun Liu, Sebastian Bauer, and Andreas Velten. Analysis of feature visibility in non-line-of-sight measurements. In *IEEE Conference on Computer Vision and Pattern Recognition*, pages 10140–10148, 2019. 2

[25] Xiaochun Liu, Ibón Guillén, Marco La Manna, Ji Hyun Nam, Syed Azer Reza, Toan Huu Le, Adrian Jarabo, Diego Gutierrez, and Andreas Velten. Non-line-of-sight imaging using phasor-field virtual wave optics. *Nature*, 572(7771), 2019. 1

[26] Tomohiro Maeda, Achuta Kadambi, Yoav Y. Schechner, and Ramesh Raskar. Dynamic heterodyne interferometry. In *IEEE International Conference on Computational Photography*, pages 1–11. IEEE, May 2018. 2

[27] Tomohiro Maeda, Guy Satat, Tristan Swedish, Lagnojita Sinha, and Ramesh Raskar. Recent advances in imaging around corners. *arXiv*, Oct 2019. 2

[28] Tomohiro Maeda, Yiqin Wang, Ramesh Raskar, and Achuta Kadambi. Thermal non-line-of-sight imaging. In *IEEE International Conference on Computational Photography*, pages 1–11. IEEE, May 2019. 2

[29] Nathan Matsuda, Oliver Cossairt, and Mohit Gupta. Mc3d: Motion contrast 3d scanning. In *2015 IEEE International*

Conference on Computational Photography, pages 1–10. IEEE, 2015. 8

[30] Wojciech Matusik, Hanspeter Pfister, Matt Brand, and Leonard McMillan. A data-driven reflectance model. *ACM Transactions on Graphics*, 22(3):759—-769, 2003. 6

[31] Daisuke Miyazaki and Katsushi Ikeuchi. Inverse Polarization Raytracing: Estimating Surface Shapes of Transparent Objects. In *IEEE Computer Society Conference on Computer Vision and Pattern Recognition*, volume 2, pages 910–917. IEEE, 2005. 2

[32] Gabriella Musarra, Ashley Lyons, Enrico Conca, Yoann Altmann, Federica Villa, Franco Zappa, Miles J. Padgett, and Daniele Faccio. Non-line-of-sight 3D imaging with a single-pixel camera. *arXiv*, Mar 2019. 1, 2

[33] Nikhil Naik, Christopher Barsi, Andreas Velten, and Ramesh Raskar. Time-resolved reconstruction of scene reflectance hidden by a diffuser. In *CLEO*, Washington, D.C., 2013. OSA. 1, 2

[34] Seung Won Oh, Ahn Ki Kim, Byung Wok Park, and Tae Hoon Yoon. Optical compensation methods for the elimination of off-axis light leakage in an in-plane-switching liquid crystal display. *Journal of Information Display*, 16(1):1–10, 2015. 2, 3

[35] Matthew O'Toole, David B. Lindell, and Gordon Wetzstein. Confocal non-line-of-sight imaging based on the light-cone transform. *Nature*, 555(7696):338–341, Mar 2018. 1, 2, 8

[36] Adithya Pediredla, Akshat Dave, and Ashok Veeraraghavan. Snlos: Non-line-of-sight scanning through temporal focusing. In *IEEE International Conference on Computational Photography*, pages 1–13. IEEE, May 2019. 1, 2

[37] Adithya Kumar Pediredla, Mauro Buttafava, Alberto Tosi, Oliver Cossairt, and Ashok Veeraraghavan. Reconstructing rooms using photon echoes: A plane based model and reconstruction algorithm for looking around the corner. In *IEEE International Conference on Computational Photography*, pages 1–12. IEEE, May 2017. 1, 2

[38] Ramesh Raskar and James Davis. 5D time-light transport matrix: What can we reason about scene properties? *MIT Technical Report*, 2008. 2

[39] Charles Saunders, John Murray-Bruce, and Vivek K Goyal. Computational periscopy with an ordinary digital camera. *Nature*, 565(7740):472–475, Jan 2019. 1, 2, 3, 4, 6, 7, 8

[40] Brandon M. Smith, Matthew O'Toole, and Mohit Gupta. Tracking multiple objects outside the line of sight using speckle imaging. In *IEEE Computer Society Conference on Computer Vision and Pattern Recognition*, pages 6258–6266. IEEE, June 2018. 2

[41] Kenichiro Tanaka, Yasuhiro Mukaigawa, Yasuyuki Matsushita, and Yasushi Yagi. Descattering of transmissive observation using Parallel High-Frequency Illumination. In *IEEE International Conference on Computational Photography*, pages 96–103, Apr 2013. 2

[42] Matthew Tancik, Guy Satat, and Ramesh Raskar. Flash photography for data-driven hidden scene recovery. *arXiv*, Oct 2018. 1

[43] Christos Thrampoulidis, Gal Shulkind, Feihu Xu, William T. Freeman, Jeffrey H. Shapiro, Antonio Torralba, Franco N. C. Wong, and Gregory W. Wornell. Exploiting occlusion in non-line-of-sight active imaging. *IEEE Transactions on Computational Imaging*, 4:419–431, 2017. 1

[44] Antonio Torralba and William T. Freeman. Accidental pinhole and pinspeck cameras: Revealing the scene outside the picture. In *IEEE Conference on Computer Vision and Pattern Recognition*, pages 374–381. IEEE, June 2012. 1, 2

[45] Tali Treibitz and Yoav. Y. Schechner. Active polarization descattering. *IEEE Transactions on Pattern Analysis and Machine Intelligence*, 31(3):385–399, 2009. 2

[46] Chia Yin Tsai, Kiriakos N. Kutulakos, Srinivasa G. Narasimhan, and Aswin C. Sankaranarayanan. The geometry of first-returning photons for non-line-of-sight imaging. In *IEEE Conference on Computer Vision and Pattern Recognition*, 2017. 1, 2

[47] Chia-Yin Tsai, Aswin C. Sankaranarayanan, and Ioannis Gkioulekas. Beyond volumetric albedo – a surface optimization framework for non-line-of-sight imaging. In *IEEE Conference on Computer Vision and Pattern Recognition*, pages 1545–1555, 2019. 1, 2

[48] Andreas Velten, Amy Fritz, Moungi Bawendi, and Ramesh Raskar. Multibounce time-of-flight imaging for object reconstruction from indirect light. In *Conference on Lasers and Electro-Optics*, Washington, D.C., 2012. OSA. 2

[49] Andreas Velten, Thomas Willwacher, Otkrist Gupta, Ashok Veeraraghavan, Moungi G Bawendi, and Ramesh Raskar. Recovering three-dimensional shape around a corner using ultrafast time-of-flight imaging. *Nature communications*, 3:745, Jan 2012. 1, 2, 8

[50] Zihao W Wang, Weixin Jiang, Kuan He, Boxin Shi, Aggelos Katsaggelos, and Oliver Cossairt. Event-driven video frame synthesis. In *Proceedings of the IEEE International Conference on Computer Vision Workshops*, pages 0–0, 2019. 8

[51] Rihui Wu, Adrian Jarabo, Jinli Suo, Feng Dai, Yongdong Zhang, Qionghai Dai, and Diego Gutierrez. Adaptive polarization-difference transient imaging for depth estimation in scattering media. *Optics Letters*, 43(6), 2018. 2

[52] Shumian Xin, Sotiris Nousias, Kiriakos N. Kutulakos, Aswin C. Sankaranarayanan, Srinivasa G. Narasimhan, and Ioannis Gkioulekas. A theory of fermat paths for non-line-of-sight shape reconstruction. In *IEEE Conference on Computer Vision and Pattern Recognition*, pages 6800–6809. IEEE, 2019. 1, 2

[53] Adam B. Yedidia, Manel Baradad, Christos Thrampoulidis, William T. Freeman, and Gregory W. Wornell. Using unknown occluders to recover hidden scenes. In *IEEE Conference on Computer Vision and Pattern Recognition*, pages 12231–12239, 2019. 1, 2, 3

[54] Xinyu Zhu, Zhibing Ge, and Shin-Tson Wu. 15.3: Analytical solutions for the wide-view lcds with uniaxial-film compensation. *SID Symposium Digest of Technical Papers*, 37(1):1071, 2006. 2, 3

[55] Alex Zihao Zhu, Nikolay Atanasov, and Kostas Daniilidis. Event-based visual inertial odometry. In *Proceedings of the IEEE Conference on Computer Vision and Pattern Recognition*, pages 5391–5399, 2017. 8